Journal of the Meteorological Society of Japan, Vol. 88, No. 3, pp. 325–347, 2010.
DOI:10.2151/jmsj.2010-305

Diurnal Variations in Lower-Tropospheric Wind over Japan Part I: Observational Results using the Wind Profiler Network and Data Acquisition System (WINDAS)

Takatoshi SAKAZAKI and Masatomo FUJIWARA

Graduate School of Environmental Science, Hokkaido University, Sapporo, Japan

(Manuscript received 24 November 2009, in final form 19 February 2010)

Abstract

This study investigates diurnal variations in lower-tropospheric wind over Japan during 2002–2008 using data from 31 stations of the Wind profiler Network and Data Acquisition System (WINDAS) and the Automated Meteorological Data Acquisition System (AMeDAS). The diurnal and semidiurnal components are extracted and analyzed to identify the dominant processes for each height range and for each season. Near the surface, the diurnal component is controlled by local wind systems (e.g., land–sea breezes) throughout the year. At 1–3 km, the diurnal component is primarily controlled by the return currents of local wind systems, with additional influence by other disturbances; the superposition of these two wind systems generates amplitude maxima in spring ($\sim$0.5 m s^{-1}) and autumn ($\sim$0.6 m s^{-1}). At 3–5 km, the diurnal wind in DJF–MAM is controlled by medium-scale eastward traveling waves, which generate the amplitude maximum ($\sim$0.8 m s^{-1}) in winter–spring. In JJA–SON, the diurnal component is controlled by a large-scale wind system with an amplitude of $\sim$ 0.3 m s^{-1}, probably related to the diurnal tide. At stations located on small islands located south of the Japanese mainland, the diurnal wind within the lower troposphere has different characteristics from those described above throughout the year. Throughout Japan, the semidiurnal wind component is controlled by the semidiurnal migrating tide above $\sim$ 1 km, and is influenced by local wind systems below $\sim$1 km. The amplitude of the semidiurnal tide below 5 km is largest in DJF ($\sim$0.4 m s^{-1}) and smallest in JJA ($\sim$0.2 m s^{-1}).

1. Introduction

Diurnal wind variations are important not only for predicting severe weather (e.g., diurnal variations in precipitation) and pollution transport, but for observing the daily-mean field. The latter means that it is essential to estimate the diurnal and subdiurnal components when observing a climatological variable with once-per-day observations (e.g., Seidel et al. 2005). In the atmosphere, diurnal wind variations are caused by several phenomena at different spatial scales; therefore, it is important to identify those processes responsible for diurnal variations at each longitude/latitude/height range and in each season.

Diurnal variations in surface wind result mainly from local-scale wind systems such as land–sea and mountain–valley breezes. Being relatively easy to measure, surface wind patterns have been reported in many previous studies conducted throughout the world (e.g., see Miller et al. 2003 for a review of studies on land–sea breezes). Sakazaki and Fujiwara (2008) recently investigated the surface wind upon Japanese plains and found that diurnal variations upon plains of 50–100 km in scale are explained mainly by the lagged combination of land–sea and mountain–valley breezes. Different types of ''local-scale'' wind systems are sometimes coupled to generate ''regional-scale'' ($\sim$100 km) wind systems (e.g., Kurita et al. 1990). In the present study, we refer to these local- and

Corresponding author: Takatoshi Sakazaki, Graduate School of Environmental Science, Hokkaido University, Sapporo, Hokkaido 060-0810, Japan.
E-mail: zaki@ees.hokudai.ac.jp

regional-scale wind systems simply as ''local wind systems''. Local wind systems are not confined to the near-surface, but extend to the upper air; return currents exist above the surface winds, thereby closing the local circulation system. The vertical scale of local circulation, including the return currents, is generally reported to be $\sim$3 km (Fujibe and Asai 1979; Tijm et al. 1999; Oliphant et al. 2001).

In the middle to upper atmosphere, variations in diurnal wind result mainly from atmospheric solar tides, which are defined as global-scale waves with periods that are harmonics of a solar day (see the review by Chapman and Lindzen 1970). Although the definition of ''global-scale'' is ambiguous, previous studies generally define the tide as diurnal and semidiurnal disturbances with zonal wavenumbers less than 6–10 (e.g., Tokioka and Yagai 1987; Lieberman and Leovy 1995; Hagan et al. 1995). Of all the tidal components, the ''migrating'' component is defined as a Sun-synchronous, westward-propagating wave (i.e., the westward-propagating diurnal (semidiurnal) component at a zonal wavenumber of 1 (2)). All other components are termed ''nonmigrating'' components. The main excitation sources of tides are the absorption of solar radiation by tropospheric water vapor and stratospheric ozone (e.g., Chapman and Lindzen 1970), as well as diurnally varying latent heat release in the tropics (Hamilton 1981; Williams and Avery 1996a; Forbes et al. 1997; Hagan and Forbes 2002, 2003). Planetary-boundary-layer sensible heating (Tsuda and Kato 1989) and solar heating of cloud particles (Sasi et al. 2001) are also possible excitation sources. Diurnal and semidiurnal tides have contrasting physical characteristics (e.g., vertical wavelength, latitudinal structure, and vertical propagation). According to tidal theory (Chapman and Lindzen 1970), the diurnal tide is dominant in the tropics and is small in midlatitudes, as vertically propagating modes are largely confined to the tropics, whereas the semidiurnal tide can propagate in all latitude regions, with a somewhat larger amplitude than that of the diurnal tide in midlatitudes.

In the upper troposphere, medium-scale eastward-traveling waves prevail, with a horizontal scale of 2000–3000 km and a zonal phase speed of 20–30 ms^{-1} (Sato et al. 1993, 2000), resulting in a period of approximately 1 day. These waves are maintained as neutral edge waves near the upper boundary in the Eady solutions (e.g., Eady 1949; Tomikawa et al. 2006, and references therein); however, the relevant excitation mechanism is poorly understood. It should be noted that in most previous studies, the frequency of medium-scale waves has been reported as approximately (not exactly) 1 day. However, Kodama et al. (2008) recently suggested that the period may be exactly 1 day, at least over East Asia, and that the excitation mechanism may be related to diurnal wind systems over the Tibetan Plateau. This proposal indicates that the medium-scale waves may be considered a disturbance that significantly contributes to diurnal variability in the upper troposphere. It should be noted that Yamamori et al. (1997) found that waves with a similar periodicity also exist in the lower troposphere, with a phase speed of $\sim$17 m s^{-1}, less than that of upper-tropospheric medium-scale waves.

As outlined above, diurnal wind variations in the troposphere are possibly influenced by local-, medium-, and global-scale wind systems, yet many previous studies have focused only on local wind systems (particularly on land–sea breezes). Few studies have provided a broader viewpoint of ''diurnal wind variations in the troposphere,'' including local wind systems. These few studies were based mainly on tropical observations, either intensive radiosonde campaigns (Tsuda et al. 1994; Alexander and Tsuda 2008) or atmospheric radars (Williams et al. 1992; Chen et al. 1996; Williams and Avery 1996b; Sasi et al. 1998, 2001; Riggin et al. 2002), and investigated the diurnal and semidiurnal wind components by focusing on atmospheric tides and local wind systems.

A smaller number of observational studies have considered diurnal wind variations in the midlatitude troposphere. In terms of the diurnal wind component, Wallace and Hartranft (1969) and Wallace and Tadd (1974) examined global-scale diurnal winds in the troposphere and lower stratosphere, using global radiosonde data. Both studies found that the diurnal wind component is affected by topography as well as by the diurnal tide; this result was later confirmed from global analysis data (Hsu and Hoskins 1989). With regard to the relationship between local wind systems and atmospheric tides, Yoshida and Hirota (1979) suggested that the diurnal wind component is influenced by local wind systems below 500 hPa and by the diurnal tide above 500 hPa, based on an analysis of radiosonde data in Japan. Fujibe and Asai (1979), using pilot-balloon and radiosonde data, showed that land–sea breezes control the diurnal wind up to $\sim$3 km upon the Kanto Plain, the largest plain

in Japan (horizontal scale of ~100 km). It should be noted that the number of stations considered in the latter two studies was less than 10 and that the period of data analysis was less than 1–2 years; these factors may be an insufficient basis upon which to draw statistically robust conclusions. In addition, in most previous studies on diurnal wind variations in the troposphere, conclusions regarding the diurnal tide were based solely on qualitative discussions; that is, wind systems with a horizontal scale greater than that of local wind systems were regarded as tides, without a quantitative estimation of their horizontal scales. Finally, the seasonality of the diurnal wind component has yet to be examined in detail.

The semidiurnal wind component in the midlatitude troposphere is caused mainly by the semidiurnal migrating tide (Wallace and Tadd 1974). This relationship was confirmed by Whiteman and Bian (1995, 1996), based on data from the wind profiler network in the USA. Sakazaki and Fujiwara (2008) confirmed a robust semidiurnal component in surface wind that is caused by the non-sinusoidal local pressure gradient force associated with local wind systems. Note that the height range up to which local wind systems control the semidiurnal wind component remains poorly understood. Likewise, seasonal variations in the semidiurnal component have yet to be examined in detail.

The goal of the present study is to investigate the detailed characteristics of diurnal wind variations over Japan, and to identify the responsible dynamical processes for each height range and for each season. A dense operational wind profiler network, the Wind profiler Network and Data Acquisition System (WINDAS), was established in Japan in 2002 to observe and predict severe rainstorms. The network, which consists of 31 stations with an average horizontal spacing of 130 km (Fig. 1), monitors 10-minute-average winds in the lower troposphere from 0.4 km up to ~5 km with a vertical resolution of ~0.3 km. Ishihara et al. (2006) reported that the average top height of wind measurements throughout the year is 5.3 km, although this value is higher in summer (6–7 km) than in winter (3–4 km). Detailed information regarding the characteristics and performance of WINDAS can be found in Ishihara et al. (2006), and the instrumentation of the wind profiler used in WINDAS is described by Hashiguchi et al. (2004). By March of 2008, 5- or 6-year continuous data sets had been compiled for most of the stations, enabling a statistical analysis of diurnal variations in upper-air winds.

The remainder of the manuscript is organized as follows. Section 2 describes data sets and analysis methods, Section 3 considers the climatological winds, and Section 4 provides two examples of diurnal wind variations. Sections 5 and 6 describe the detailed characteristics of the diurnal and semidiurnal wind components, respectively, and discuss the controlling processes for each component. Finally, the main findings of the study are summarized in Section 7. In Part II of this study (Sakazaki and Fujiwara 2010), the dynamical processes that control the observed diurnal wind component, as described in the present paper (Part I), are further examined based on Japanese Meteorological Agency (JMA) meso-scale analysis data (MANAL) and four global reanalysis data sets.

2. Data and analysis methods

WINDAS, operated by the JMA, consists of 31 1.3 GHz wind profilers (see Fig. 1 for station locations). Most of the stations are located in coastal areas of the four main Japanese islands (Hokkaido, Honshu, Shikoku, and Kyushu; hereafter, these areas are collectively referred to as the ''main Japanese islands''), with three stations located on small islands located south of the Japanese mainland within the Pacific (hereafter referred to as ''small southern islands''). On the main Japanese islands, the surface wind is expected to be influenced mainly by land–sea breezes. In the present study, measurements are made in terms of the height from the ground at each station, with a vertical resolution of ~0.3 km. Note that because the altitude of the ground level at most WINDAS stations is less than 50 m above sea level, we did not take into account differences among the stations in terms of measurement altitude; thus, the height from ground level is simply referred as ''height.'' Every 10 minutes, 10-minute averages of three wind components (u: eastward wind, v: northward wind, w: vertical wind) over each wind profiler station are calculated from Doppler velocities. Measurements have been taken since April 2002 for 25 stations and since March or June 2003 for the other 6 stations. We analyze the data set for the 5- or 6-year periods until March 2008.

At the WINDAS stations, surface winds are monitored using the Automated Meteorological Data Acquisition System (AMeDAS), which is also operated by JMA. We analyze 10-minute aver-

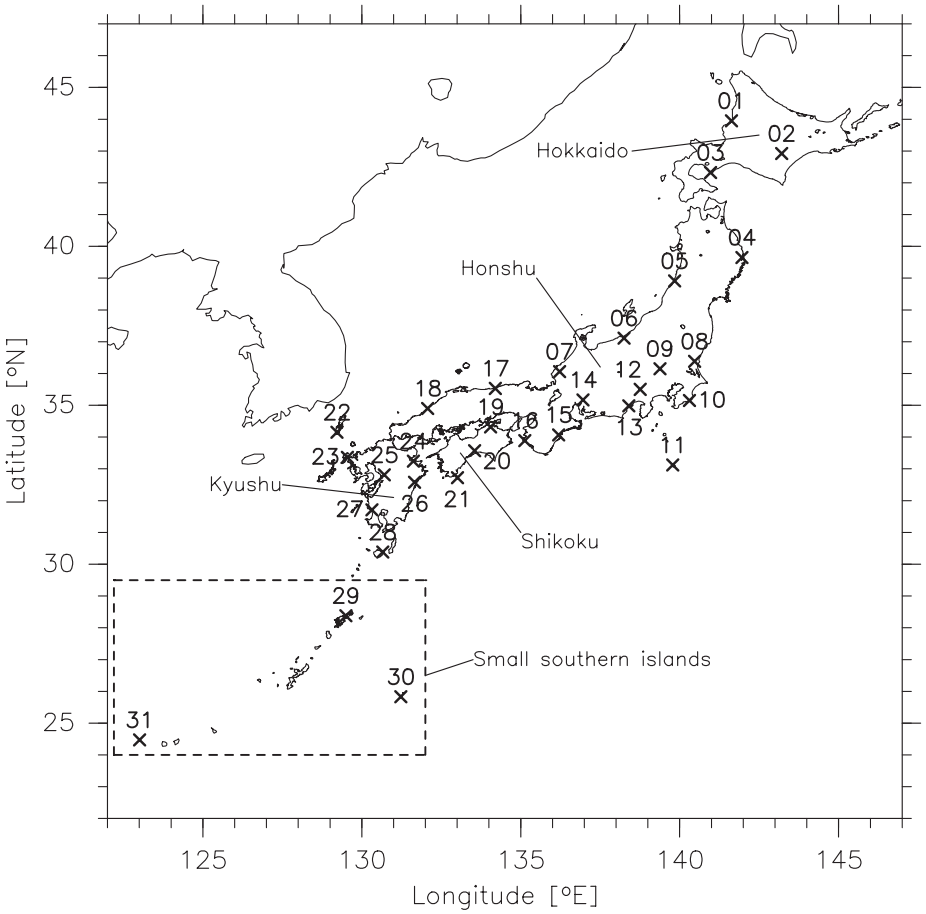

Fig. 1. Map of Japan showing the location of WINDAS stations (crosses). The numbers beside the crosses are station numbers. "main Japanese islands" refers to Hokkaido, Honshu, Shikoku, and Kyushu. The islands within the dashed rectangle are referred to as "small southern islands" in this study. In this region, 1° of longitude corresponds to ~90 km.

age data of surface wind velocity collected every 10 minutes, as for the WINDAS data, for the period from April 2002 to March 2008. In the following sections, the data at the surface (0.0 km) are AMeDAS data.

Given the occurrence of missing data, particularly in WINDAS data, we first produced a hourly data set by calculating a seven-point running average of 10-minute data around each hour, for both WINDAS and AMeDAS data (i.e., the data at 6:00 is the average of the seven points from 5:30 to 6:30). We calculated the average in all cases with at least one valid datum among of seven time points. Figure 2 shows the percentage of valid hourly data for WINDAS in December–January–February (DJF), March–April–May (MAM), June–July–August (JJA), and September–October–November (SON). There are few missing data (less than 20%) below 2 km for the hourly data throughout the year. Above 2 km, however, the rate of data acquisition shows a rapid decrease with height, except for JJA. In this study, we used data for heights below 5.1 km, regardless of the month. The acquisition rate for AMeDAS data exceeds 99% for all seasons (data not shown).

The procedures employed in data processing and analysis for the hourly WINDAS and AMeDAS data are as follows. At each station, the hourly, local-time composite winds (u and v) are calculated for each height and for each month. For each monthly-composite data set, we use the data for three months (e.g., the composite data for January are constructed with December–January–February data). We average all the available data in obtain-

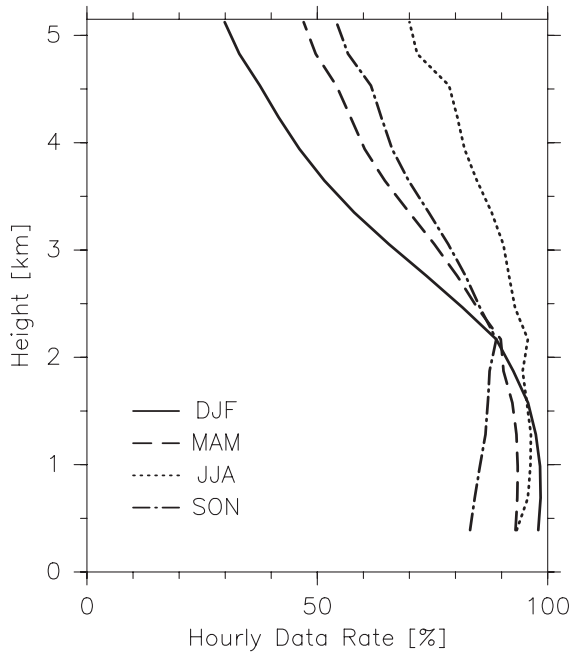

Fig. 2. Proportion of hourly data used for the composite analysis with respect to all data, including missing data. The average for all stations is shown. The solid curve is for December–January–February (DJF), dashed curve for March–April–May (MAM), dotted curve for June–July–August (JJA), and dot-dashed curve for September–October–November (SON).

ing the composite. The results do not change in the case that we omit days when typhoons cross Japan ($\sim$60 cases during the 6 years of interest). Using this data set, the hourly anomaly wind is extracted from the 24-hour mean. Next, using a Fourier transform, the diurnal and semidiurnal components (i.e., their amplitudes and phases) are calculated. The phase is represented by the local time when each component (u and v) attains its maximum. Wind measurements were conducted in Japanese Standard Time (JST), which is defined at (35°N, 135°E). The WINDAS/AMeDAS network ranges between $\sim$125°E and $\sim$145°E (Fig. 1), which corresponds to a maximum time difference of $\sim$1 hr. The phases are corrected to the actual "local" solar time (LT) at each station depending on the longitude.

We also calculate the standard errors (SE) in the amplitudes and phases of the diurnal and semidiurnal components. Note that SE is different from the standard deviation (SD): SE represents the error in the composite estimation, whereas SD represents the degree to which individual data on each day deviate from the composite value. The procedure employed in calculating SE is as follows. We assume that the deviation of each original hourly datum (i.e., hourly data before performing the composite analysis) from the monthly composite value is caused by random errors. Based on this assumption, the unbiased variance (σ^2) about the composite value at each local time is calculated; subsequently, σ is obtained for the amplitudes and phases of the diurnal and semidiurnal components, following error propagation theory. Finally, we obtain SE, defined as $\sigma/\sqrt{n-1}$, where n is the total number of hourly data for each station, each height, and each month. Because the diurnal (semidiurnal) phase takes values between 0000 LT and 2400 (1200) LT, phase data with SE greater than 12 (6) hr are not plotted in Figs. 6c–d, 11, or 14c–d.

In addition to WINDAS and AMeDAS data, four-times-daily Japanese reanalysis data (JRA25 and JMA Climate Data Assimilation System (JCDAS); hereafter referred to as JRA25) (Onogi et al. 2007) are used to assess climatological winds over Japan (Section 3), for the 6-year analysis period from April 2002 to March 2008.

Finally, output data from the Global Scale Wave Model (GSWM02) (Hagan et al. 1995, 1999; Hagan and Forbes 2002, 2003) are compared with our results as a reference for atmospheric tides. GSWM02 is a two-dimensional, linearized, steady-state numerical tidal and planetary wave model that covers the height region from the ground to the thermosphere. This model only calculates the diurnal and semidiurnal tides at zonal wavenumbers from -6 to 6, based on the assumption that each zonal wavenumber component behaves independently from the others. Regarding the excitation sources for the tides, radiative heating of ozone and water vapor are considered for the migrating component, while latent heat release in the tropics is considered for both the migrating and nonmigrating components; topography and sensible heat flux in the boundary layer are not taken into account. The horizontal spacing of the output data is $5° \times 5°$, with a vertical resolution of 4 km. Here, we only consider data at a height of 4 km.

3. Climatological winds

Before examining diurnal variations, we investigate climatological winds in the lower troposphere

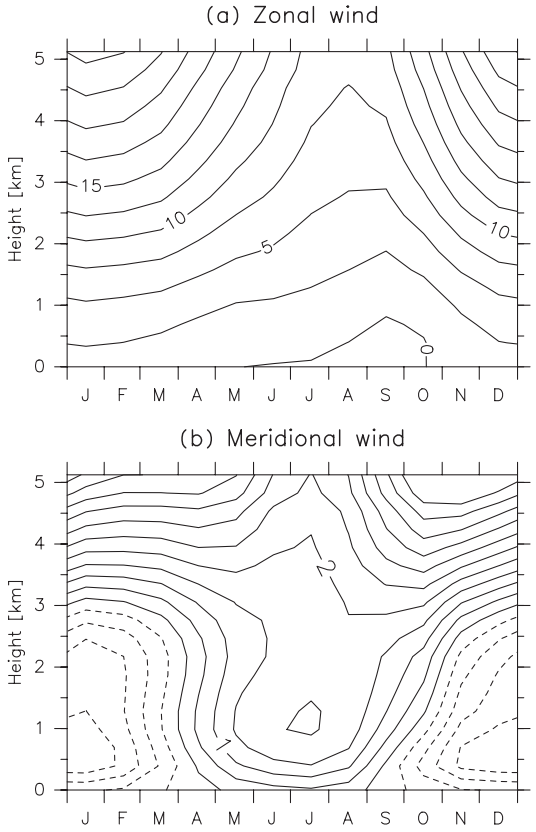

Fig. 3. Month–height distributions of daily-mean (a) zonal wind and (b) meridional wind averaged for all stations. The contour interval is 2.5 m s^{-1} for (a) and 0.5 m s^{-1} for (b). For (b), solid and dashed lines show northward and southward winds, respectively.

over Japan. Figure 3 shows month–height distributions of the observed daily-mean zonal and meridional winds averaged for all WINDAS stations. We found only minor inter-station differences (data not shown). Zonal wind is eastward throughout the year, with its speed increasing with height and attaining a maximum in winter. The meridional wind behavior is different above and below 3 km: above 3 km, the wind is northward throughout the year and reaches a maximum in winter, whereas below 3 km the wind is southward in winter and northward in summer.

The above features are also evident in global reanalysis data. Figure 4 shows climatological JRA25 horizontal winds at 925 and 500 hPa in DJF and JJA. The subtropical jet prevails at 500 hPa over Japan, and is stronger in DJF than in JJA (Figs. 4b and 4d). In DJF at 925 hPa (Fig. 4a), the wind is blowing from the Siberian high-pressure system on the Eurasian Continent, which develops due to radiative cooling. The location of this high explains the wintertime southward winds near the surface over Japan (Fig. 3b). In DJF at 500 hPa (Fig. 4b), Japan is located downstream of a climatological trough within the subtropical jet, probably due to the topographic effects of the Tibetan Plateau (Held 1983). At this time, a large gyre occurs in the western Pacific to the south of Japan, representing a dynamical response to diabatic heating in the tropics, known as the Matsuno–Gill pattern (Matsuno 1966; Gill 1980). Thus, the northward winds at 3–5 km in winter (see Fig. 3b) are caused by a combination of the meandering subtropical jet and the gyre due to the Matsuno–Gill pattern. In JJA at both 925 hPa (Fig. 4c) and 500 hPa (Fig. 4d), Japan is located in the western part of the Ogasawara (Bonin) high pressure system over the northwestern Pacific Ocean; the wind is northward at both 925 and 500 hPa over Japan (Fig. 3b).

4. Examples of variations in diurnal and semidiurnal wind

In this section, we provide examples of diurnal wind variations recorded at small southern islands and on the main Japanese islands in summer. Figure 5a shows the time–height distributions of hourly anomaly meridional wind at Minamidaitojima (station 30 in Fig. 1) and at Kumagaya (station 9 in Fig. 1) in JJA. Minamidaitojima is a small island of just $\sim$6 km across, whereas Kumagaya is located upon the Kanto Plain, the largest plain in Japan, and is strongly influenced by local wind systems (regional-scale land–sea breezes) (e.g., Kurita et al. 1990). Figure 5b and 5c shows the diurnal and semidiurnal components of v, respectively, as extracted from the anomaly winds in Fig. 5a. Figure 5d shows diurnal variations reconstructed from the diurnal and semidiurnal components only. At both stations, these two components perform well in reproducing the detailed features of the original variations in Fig. 5a.

At Minamidaitojima, the distribution with all components basically shows a vertically standing structure throughout the region. The diurnal and semidiurnal wind components also show a standing structure, and the diurnal amplitude ($\sim$0.4 m s^{-1}) is larger than the semidiurnal amplitude ($\sim$0.2 m s^{-1}).

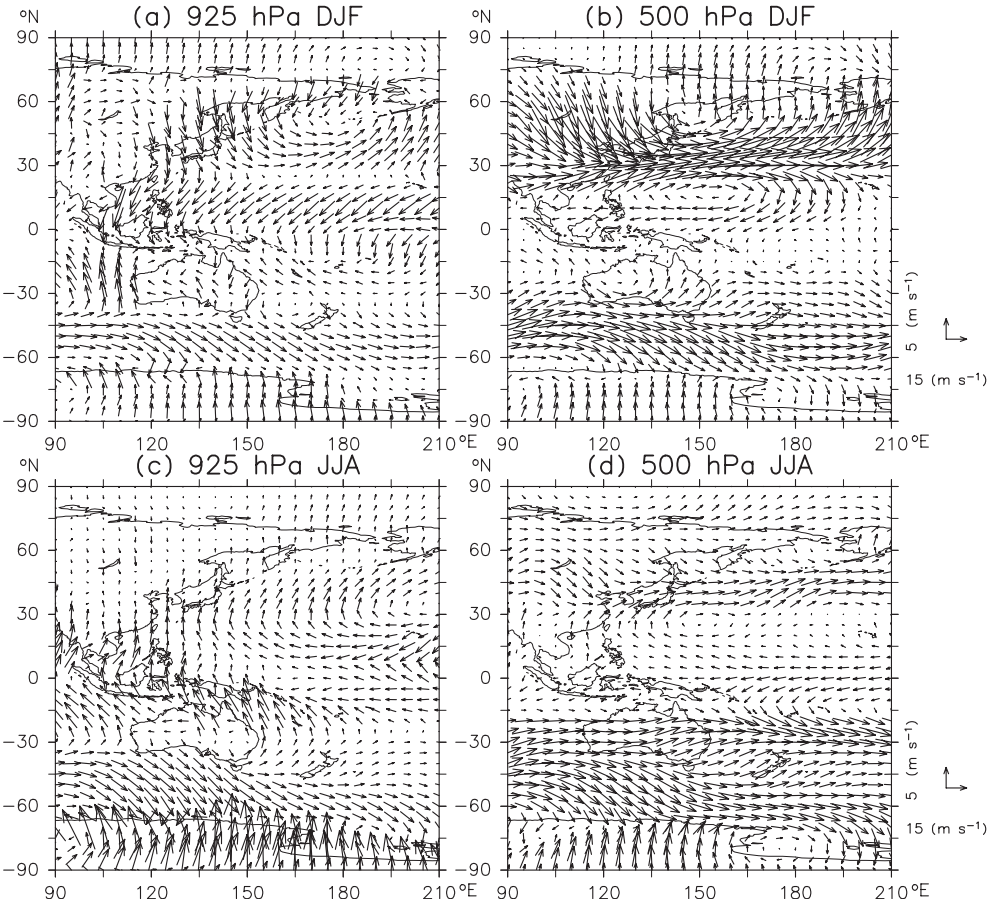

Fig. 4. Climatological horizontal winds derived from JRA25 data for the period from April 2002 to March 2008. (a) and (b) are for 925 and 500 hPa, respectively, in December–January–February (DJF). (c) and (d) are for 925 and 500 hPa, respectively, in June–July–August (JJA). Reference vectors are shown on the right-hand side.

At Kumagaya, the characteristics are markedly different from those at Minamidaitojima. We observe a clear phase reversal at around 1.5 km. The lower oscillation is centered at 0.5 km and the upper oscillation is vertically elongate, with the amplitude of the former being slightly larger than that of the latter. The harmonic components show that the diurnal amplitude (0.6–1.2 m s^{-1}) is larger than the semidiurnal amplitude (0.1–0.3 m s^{-1}) throughout the region. The phase reversal evident at around 1.5 km in Fig. 5a is clearly represented in the diurnal component. Note that above this level, the phase of the diurnal component is generally consistent between Kumagaya and Minamidaitojima. The semidiurnal component also shows a vertically standing structure above 2 km. The vertical structure and the phase at Kumagaya are basically similar to those at Minamidaitojima throughout the height region, although a phase distortion appears at $\sim$0.5 km, which is lower than the phase reversal in the diurnal component. These findings suggest that for both the diurnal and semidiurnal wind components, Minamidaitojima and Kumagaya are fundamentally influenced by a common, large-horizontal-scale wind system, at least above 2 km, and that at Kumagaya below 2 km, local wind systems are dominant over the large-scale wind system.

5. Results and discussion on the diurnal wind component

Here, we analyze the diurnal wind component at all stations. In Section 5.1, we examine the overall features of vertical profiles and seasonal variations;

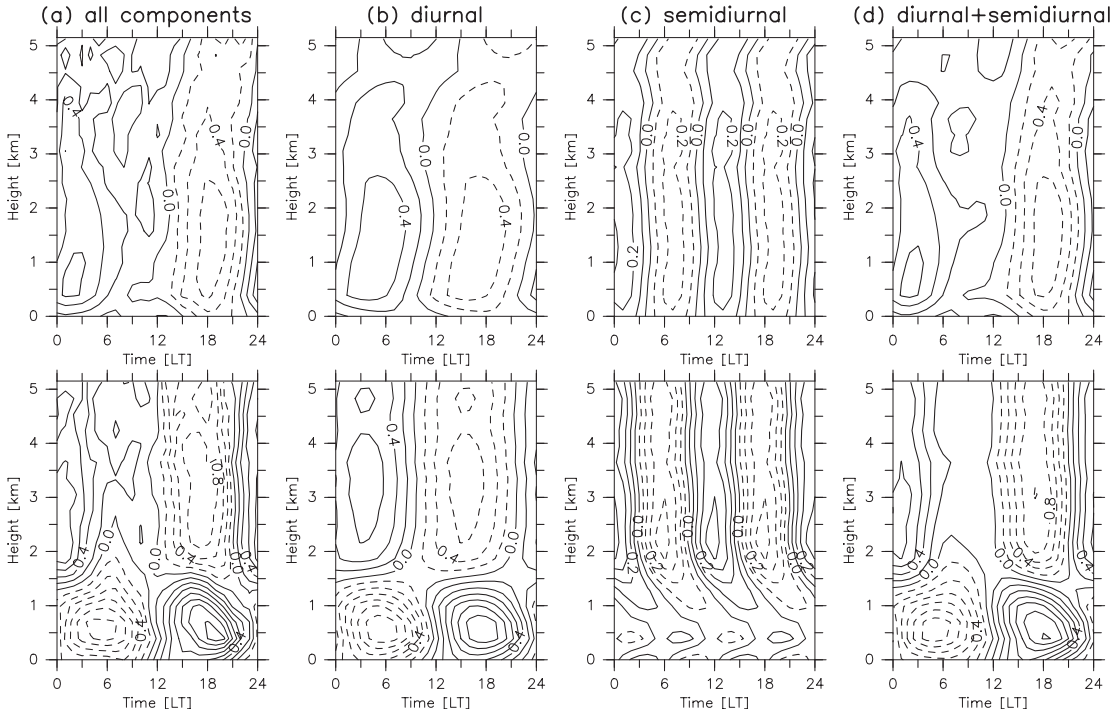

Fig. 5. Time–height distributions of variations in diurnal meridional wind in June–July–August at (top) Minamidaitojima and (bottom) Kumagaya (stations 30 and 9 in Fig. 1, respectively). (a) Hourly anomaly variations including all components, (b) diurnal component, (c) semidiurnal component, and (d) variations reconstructed from the diurnal and semidiurnal components only. The contour interval is 0.2 m s^{-1} for (a), (b), and (d), and 0.1 m s^{-1} for (c). Surface data are from AMeDAS.

spatial inhomogeneities are considered in Section 5.2. In Section 5.3, we further examine the return currents and the eastward-traveling phenomena, which are introduced in Section 5.2.

5.1 Overall features of vertical profiles

Figure 6 shows vertical profiles of the diurnal amplitude at 31 WINDAS stations for each season; the average values for all stations are also shown. The average amplitudes are 0.3–0.5 m s^{-1} throughout the year, except for a maximum of 0.7–0.8 m s^{-1} near the surface, where SD is also large ($\sim$0.5 m s^{-1}). Secondary peaks appear at 1–3 km in JJA and SON: u has a secondary peak at $\sim$2 km (1.5 km) in JJA (SON), while v has a secondary peak at $\sim$2 km (3 km) in JJA (SON). These peaks occur because large secondary peaks are observed at some stations at 1–3 km (thin lines; see also Fig. 5b, in which a secondary peak is seen at 2–4 km at Kumagaya). It should be noted that differences among the stations decrease with height, particularly in JJA and SON. For example, the SD of v in JJA–SON is $>$0.2–0.3 m s^{-1} below $\sim$3 km, but is $<$0.2 m s^{-1} above $\sim$3 km. We suggest that a large-scale wind system influences the diurnal wind component above $\sim$3 km during JJA–SON. These features are unclear in DJF and MAM.

Figure 7 shows the month–height distributions of diurnal amplitude averaged for all stations. A t-test is used to assess statistically significant deviations from the yearly average amplitude. Here we assume that the difference in the value at each station from the station average is caused by random errors. Three marked seasonal characteristics are found in different height regions. First, near the surface, below $\sim$1 km, the amplitude is largest ($\sim$1 m s^{-1}) from spring to autumn for both u and v. We propose that this broad peak results from local wind systems that develop mainly in summer due to weak background winds. Second, in the height region of 1–3 km, the amplitude attains maxima in autumn ($\sim$0.6 m s^{-1}) and spring ($\sim$0.5 m s^{-1}). The amplitudes of these maxima are larger for v than for u. Large secondary peaks in amplitude

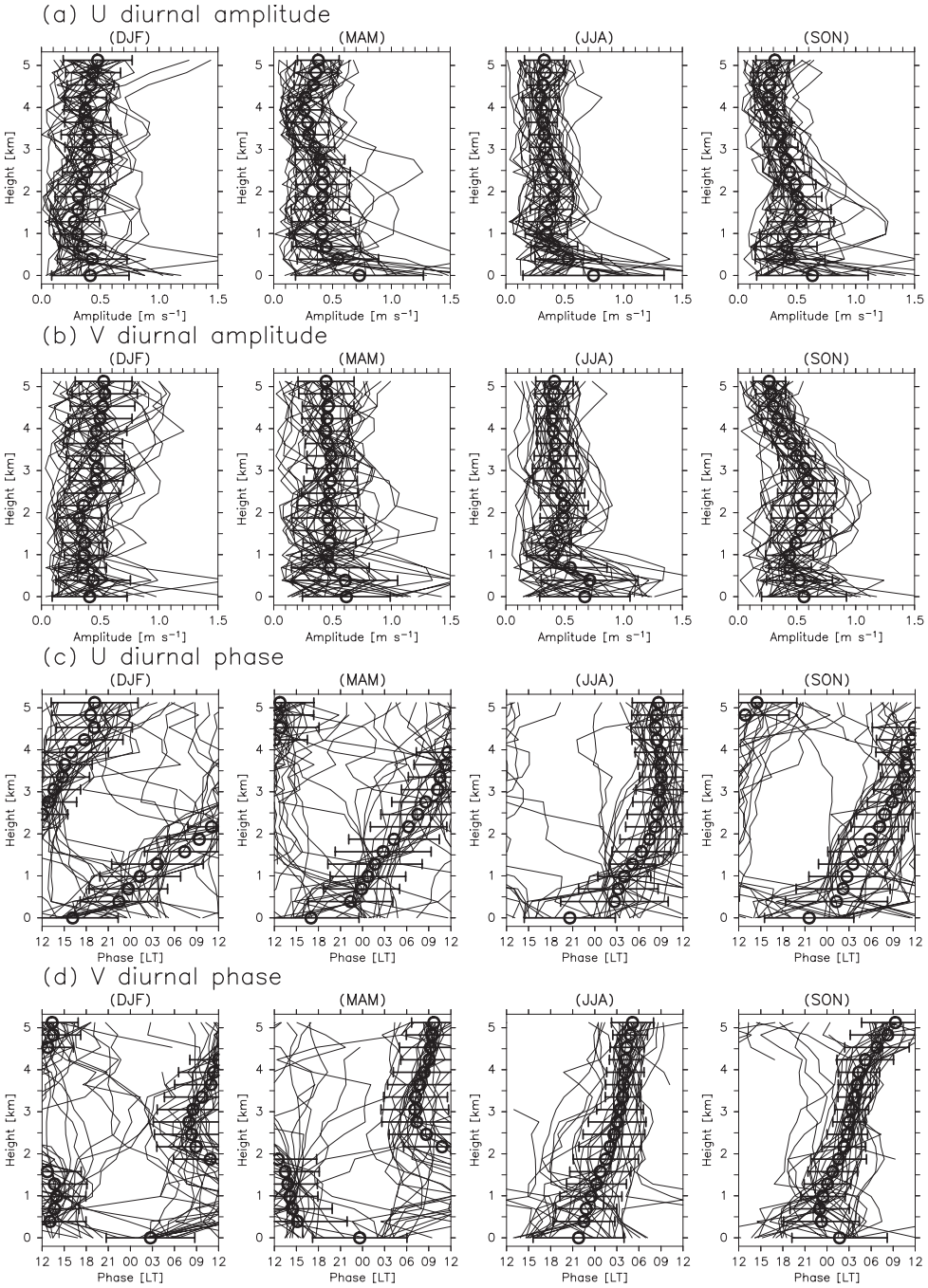

Fig. 6. Vertical profiles of the amplitude and phase of the diurnal component in December–January–February (DJF), March–April–May (MAM), June–July–August (JJA), and September–October–November (SON). (a) Diurnal amplitude of zonal wind, (b) diurnal amplitude of meridional wind, (c) diurnal phase of zonal wind, and (d) diurnal phase of meridional wind. Thin lines are profiles at individual stations. Solid circles and horizontal bars are the average and SD, respectively, for all stations. For (c) and (d), data are not plotted in the case that the standard error exceeds 12 hr.

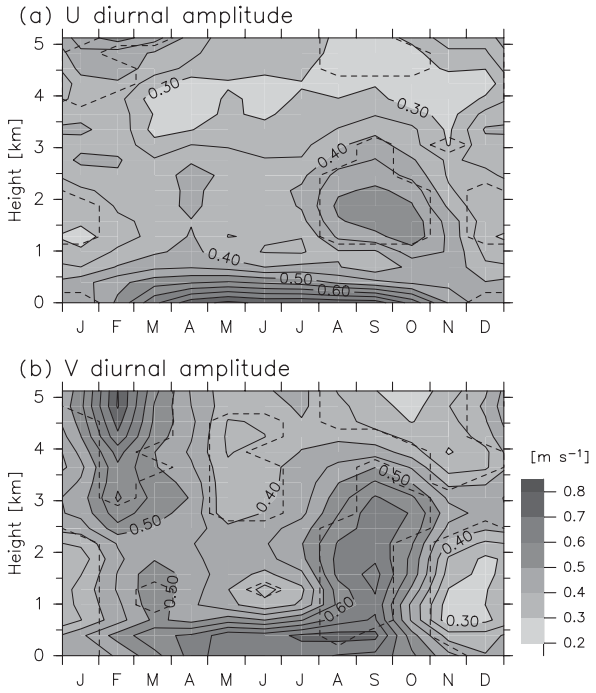

Fig. 7. Month–height distributions of the diurnal amplitude averaged for all stations, showing (a) the zonal component and (b) the meridional component. The contour interval is 0.05 m s^{-1}. Regions surrounded by dashed curves represent statistically significant regions (95% level, t-test).

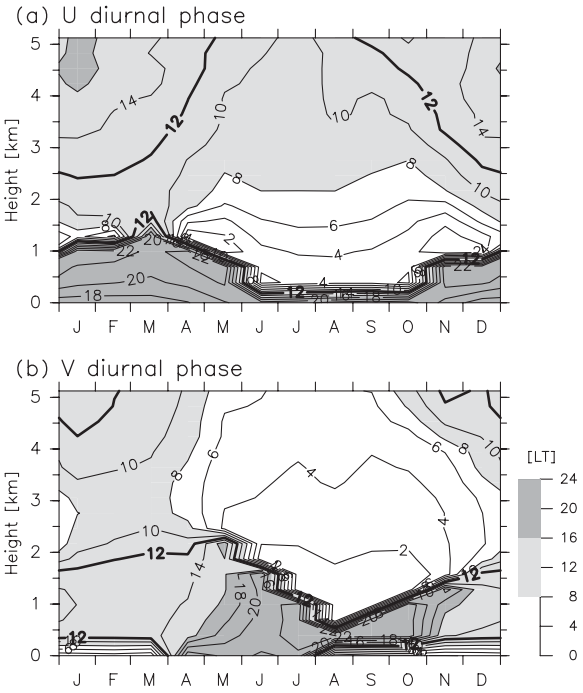

Fig. 8. As for Fig. 7, but for the diurnal phase averaged for all stations. The contour interval is 2 hr.

occur at some stations at heights of 1–3 km (see Fig. 6a and 6b). Finally, above 3 km, the amplitude reaches a maximum in February, with clearer signals in v ($\sim$0.8 m s^{-1}) than in u. The amplitude in v is as large as that near the surface.

Figure 6 also shows vertical profiles of diurnal phases for each season. Here, the station-average phase is defined as the phase of the diurnal component extracted from the hourly anomaly components averaged for all stations. Because the phases associated with local wind systems are expected to be canceled out when taking the station average, the average phase is expected to be due to larger-scale phenomena, at least as large as the scale of the Japanese Archipelago (>1000–1500 km). The average phase of u has a positive slope below $\sim$2 km and is nearly constant with height above $\sim$2 km throughout the year. The average phase of v is nearly constant with height in DJF and MAM, and the phase near the surface is preceded by that in upper air regions. The average phase of v in JJA and SON has a small positive slope with height. A typical example is seen at Minamidaitojima in JJA (Fig. 5a). Note that the differences among stations decrease with height, particularly in JJA, as also seen in amplitude (Figs. 6a, b). In fact, the SD of v in JJA is $\sim$6 hr below 3 km, but <3 hr above 3 km. In other seasons, the SD of v in upper air regions (3–5 hr) is also smaller than that at the surface (>6 hr), although SD in upper air regions is larger than that in JJA. These findings are consistent with the data shown in Figs. 6a, b, which indicate that a larger-scale wind system influences the diurnal component above $\sim$3 km, particularly in JJA.

Figure 8 shows the month–height distributions of the diurnal phase averaged for all stations. A clear seasonal variation in phases is found for the entire region. In DJF, the average phase of u is $\sim$2100 LT at 1 km, becoming later with increasing height to $\sim$1500 LT at 4 km (see also Fig. 6). In JJA, in contrast, the phase is $\sim$0300 LT at 1 km and $\sim$0900 LT at 4 km. The phase changes drastically at around April–May and around November–December. A marked seasonal variation is also seen for v: in DJF the phase is $\sim$1500 LT at 1 km and $\sim$1200 LT at 4 km, whereas in JJA the phase

at 1 km is ~0000 LT, becoming later with height to ~0400 LT at 4 km. Again, the phases change drastically during the same months in which a change is seen in u. Given that the phase of local wind systems is not expected to change considerably during the year (see Fig. 10, for 0.0 km), these findings suggest that the dominant large-scale phenomena differ between DJF–MAM and JJA–SON.

5.2 Spatial inhomogeneity

Here, we examine spatial inhomogeneity in the diurnal wind component. An appropriate way to illustrate the horizontal distribution of the characteristics of diurnal wind variations is to use hodographs and harmonic dial vectors. The hodograph represents diurnal variations in the wind vector at a given point. Details of the method employed in analyzing hodographs can be found in Sakazaki and Fujiwara (2008). The harmonic dial vector represents the amplitude and phase of any harmonic component based on its length and direction, respectively. Figures 9 and 10 show hodographs of the diurnal wind component and the harmonic dial vectors of the diurnal component of v, respectively, at 0.0, 1.9, and 5.1 km in DJF, MAM, JJA, and August–September–October (ASO). These three height levels correspond to the levels where distinct seasonal variations are found in diurnal amplitudes (see the previous section and Fig. 7). For harmonic dial vectors, we show the results for v because most WINDAS stations are located near the coast, which is approximately oriented east–west (Fig. 1); consequently, the effects of local wind systems (land–sea breezes) are seen more clearly in v than in u. In the following sub-sections, we examine in detail the spatial characteristics of the diurnal wind component for the main Japanese islands (Sections 5.2.a–c) and for stations located on small southern islands (stations 29–31; herein referred to as I-stations) (Section 5.2.d).

a. At the surface (0.0 km height) for the main Japanese islands

At the surface (0.0 km) for the main Japanese islands, most of the hodographs are elongate in a direction crossing the local coast (Figs. 9, 10). In addition, the winds are basically offshore during the nighttime (~0300 JST) and onshore during the daytime, indicating that the winds are controlled mainly by land–sea breezes. Some of the hodographs show an anticlockwise rotation, indicating that the surface winds are also influenced by mountain–valley (mountain–plain) breezes (Sakazaki and Fujiwara 2008). The amplitudes are largest in JJA and smallest in DJF, whereas the phases show no marked change during the year.

b. At 1.9 km height for the main Japanese islands

Here, we examine the diurnal component at 1.9 km height for the main Japanese islands. In JJA, the direction of the wind vector at 0000 LT is basically onshore (Fig. 9), and the diurnal component of v attains a maximum at ~1800 LT (~0400 LT) along the north (south) coast (Fig. 10). These findings indicate that the winds are basically onshore (offshore) during the nighttime (daytime) and that the phases are approximately opposite those at 0.0 km. Therefore, it is suggested that the return currents of the local wind system prevail at this height in JJA. In addition, the spatial differences among hodographs (e.g., direction of the major axis) are smaller at 1.9 km than at 0.0 km. For example, the large difference in the major axes of hodographs among stations 08, 09, 12, and 13 at 0.0 km is not seen at 1.9 km. It is inferred that the return currents have a larger horizontal scale than do the surface winds; that is, they are not as sensitive to complex (or "local") coastlines as are the surface winds.

In ASO, similar features are observed to those in JJA; however, a salient feature in ASO is that the winds along the south coast (e.g., stations 8–10 and 12–16) have larger amplitudes (~1 m s^{-1}) than those in JJA, contributing to the autumn maximum in amplitude at 1–3 km (Fig. 7). In fact, the diurnal amplitude of v averaged for the stations along the south coast (stations 2, 3, 9, 10, 12–16, 20, and 21; herein referred to as S-stations) in ASO is ~0.8 m s^{-1}, which is ~0.2 m s^{-1} larger than the average for all stations in ASO (Fig. 7). It can be inferred that the return currents are basically proportional to the strength of the surface wind system. Considering that the surface winds in ASO are almost the same as those in JJA (Fig. 9), it is suggested that other disturbances are superposed on the return currents, resulting in larger amplitudes along the south coast in ASO.

In MAM, the return currents are discernible as a phase contrast between the north and south coasts of the main Japanese islands (Fig. 10). Furthermore, the winds along the north coast (e.g., stations 5–7 and 17–18) have larger amplitudes (~1 m s^{-1}) than those in JJA, particularly for v. In contrast, the amplitudes of return currents along the south coast in MAM are much smaller than those in JJA

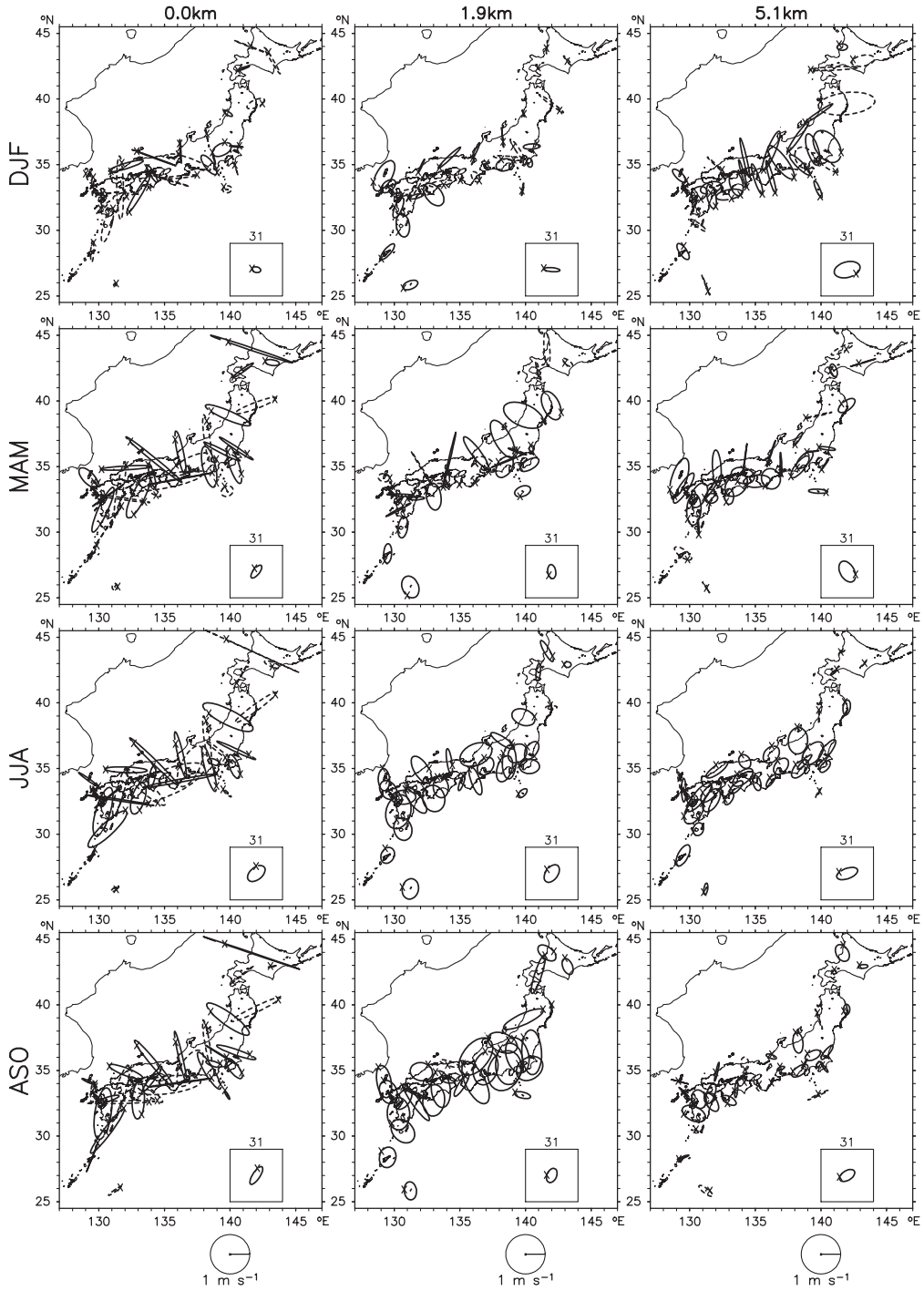

Fig. 9. Hodographs reconstructed from the diurnal component for (top) December–January–February (DJF), (upper middle) March–April–May (MAM), (lower middle) June–July–August (JJA), and (bottom) August–September–October (ASO), and for heights of (left) 0.0 km, (center) 1.9 km, and (right) 5.1 km. The hodograph at station 31 is shown in the small square within each panel. Solid and dashed ellipses represent clockwise and anticlockwise rotations, respectively. The symbol X in each hodograph denotes the head point of the wind vector at 0000 LT. Reference hodographs are shown at the bottom of the figure.

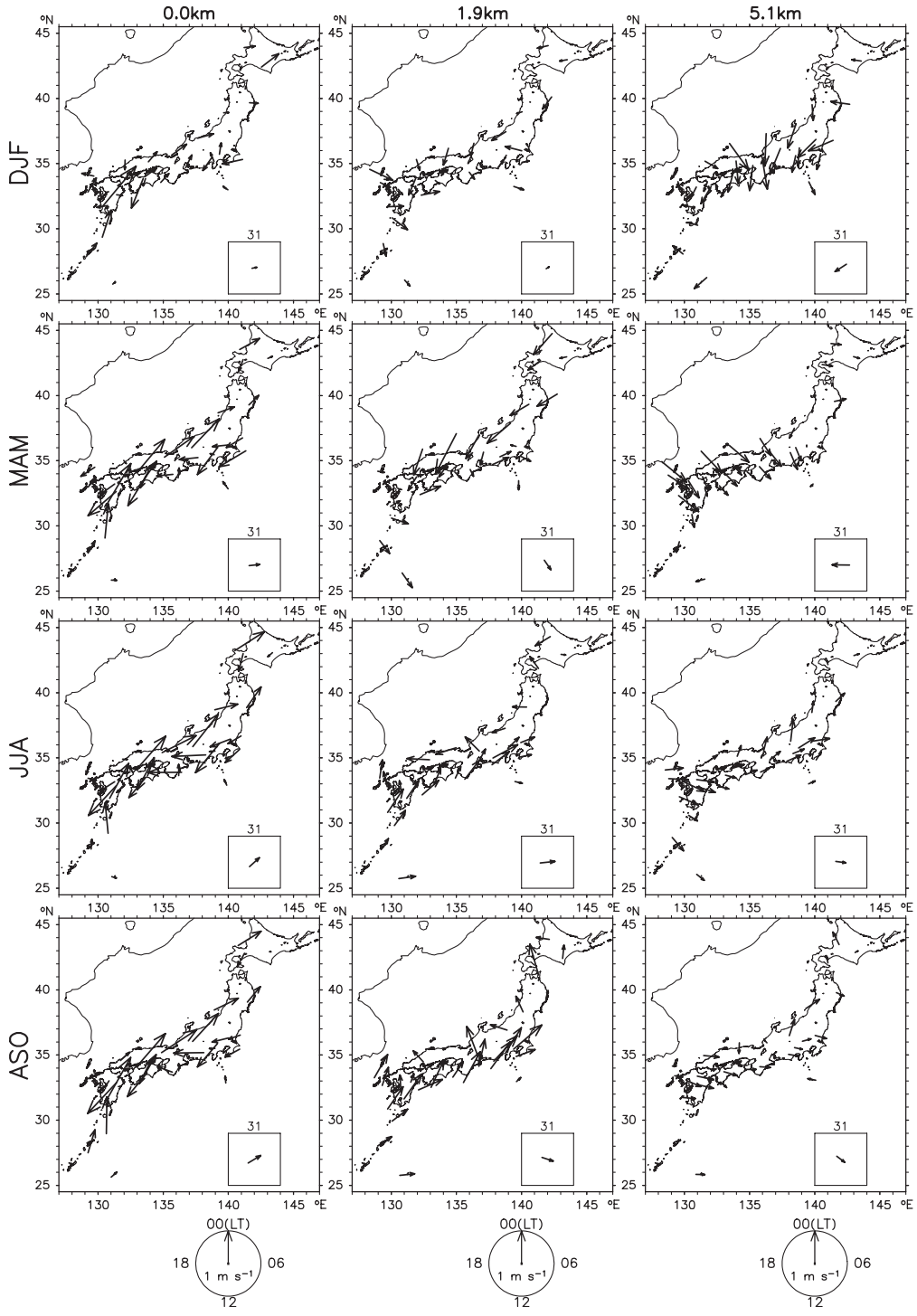

Fig. 10. As for Fig. 9, but for harmonic dial vectors of the diurnal component of v. Reference harmonic dial vectors are shown at the bottom of the figure.

and ASO (Fig. 10). The large amplitudes along the north coast contribute to the spring maximum in amplitude at 1–3 km in MAM (Fig. 7). The diurnal amplitude of v averaged for stations along the north coast (stations 5–7 and 17–19; herein referred to as N-stations) in MAM is $\sim$1.0 m s^{-1}, twice as large as the average for all stations in MAM (Fig. 7). In addition, the amplitudes at 0.0 km are smaller in MAM than in JJA. It is inferred that in MAM also, other disturbances are superposed on the return currents, resulting in large amplitudes along the north coast.

Finally, in DJF, the wind pattern is similar to that in MAM, although with a smaller amplitude, especially along the south coast. The phase along the north coast in DJF is increasingly delayed toward the east (Fig. 10). For example, the phases at stations 22, 07, and 06 are $\sim$0800 LT, $\sim$1200 LT, and $\sim$1700 LT, respectively. A similar phase delay is seen in MAM along the north coast (Fig. 10): the phases at stations 18 and 05 are $\sim$1300 LT and $\sim$1600 LT, respectively. This type of phase delay along the north coast is only seen in DJF–MAM. These findings suggest that in DJF and MAM, eastward-moving phenomena prevail over Japan at 1.9 km height. These eastward-moving signals are further investigated in Section 5.3.b.

c. At 5.1 km height for the main Japanese islands

Finally, we examine the diurnal component at 5.1 km height for the main Japanese islands. In DJF, the winds have larger amplitudes than those in JJA and the hodographs are elongate in a north–south orientation (Fig. 9). This finding indicates that the amplitudes of v are larger than those of u in DJF, as shown in Fig. 7. The phase of v is basically $\sim$1200 LT (Fig. 10). It should be noted that a clear eastward phase delay is observed over Honshu ($\sim$35°N). For example, the phases at stations 18, 07, and 08 are $\sim$0900 LT, $\sim$1200 LT, and $\sim$1800 LT, respectively. At these stations, the amplitudes reach $\sim$1.0 m s^{-1}, resulting in large amplitudes in winter at 3–5 km height (Fig. 7). For the diurnal component of u, an eastward delay at 5.1 km is observed only around 40°N (stations 1–5). In other areas of the main Japanese islands, the phases of u are different between stations located along the north coast (1200–1800 LT) and those along the south coast (1900–0000 LT) (data not shown), in contrast to the features in JJA.

In JJA, the diurnal winds at 5.1 km height are blowing coherently at almost all stations; the differences among stations are small compared with those at 0.0 or 1.9 km, as noted in Sec. 5.1 and as shown in Fig. 6. These features are also seen in the harmonic dial vectors in u (data not shown). The phase of v over the main Japanese islands is 0000–0600 LT (Fig. 10), and that of u is 0600–1200 LT (data not shown, but see Fig. 6). These values are somewhat different from those in DJF. The amplitudes are $\sim$0.3–0.4 m s^{-1}, smaller than those in DJF. In addition, unlike in DJF, the eastward phase delay is not observed. These findings suggest that a large-scale wind system, with a horizontal scale of at least $\sim$3000 km, controls the diurnal wind component at 5.1 km height in JJA and that this wind system is different to the system that prevails in DJF. This wind system is hereafter referred as the diurnal tide, as it is identified as such in Part II of this study.

The wind patterns in MAM and SON are similar to those in DJF and JJA, respectively. This result corresponds to the findings presented in Sec. 5.1 (see Fig. 8), whereby the wind pattern shows drastic changes in May–June and in November–December.

d. Stations located on small southern islands

Finally, we examine the diurnal wind component at the I-stations. At the surface, the amplitudes are $\sim$0.2 m s^{-1} throughout the year, much smaller than the values recorded throughout the main Japanese islands. This finding suggests that local wind systems do not develop at these island stations. The phases of v are 0300–0600 LT, with little seasonal variation. At 1.9 km, the amplitudes are a little larger (0.1–0.2 m s^{-1}) than at the surface throughout the year. The phases of v are 0900–1200 LT in DJF and 0300–0600 LT in JJA (Fig. 10). At 5.1 km, the amplitudes are $\sim$0.2–0.4 m s^{-1} and the phases are 1500–1800 LT in DJF and 0600–0900 LT in JJA, showing a seasonal variation.

In addition, in DJF at both 1.9 and 5.1 km height, the phases are only consistent with those over the southern part of Kyushu (stations 27 and 28), where the eastward phase delay is not observed. In JJA, the phases at 1.9 km are close to those at stations along the south coast of the main Japanese islands, and the phases at 5.1 km are similar to those for almost all stations over the main Japanese islands.

At both 1.9 and 5.1 km, the features in MAM (SON) are similar to those in DJF (JJA) (see Fig. 11). An analysis of u at island stations yields similar

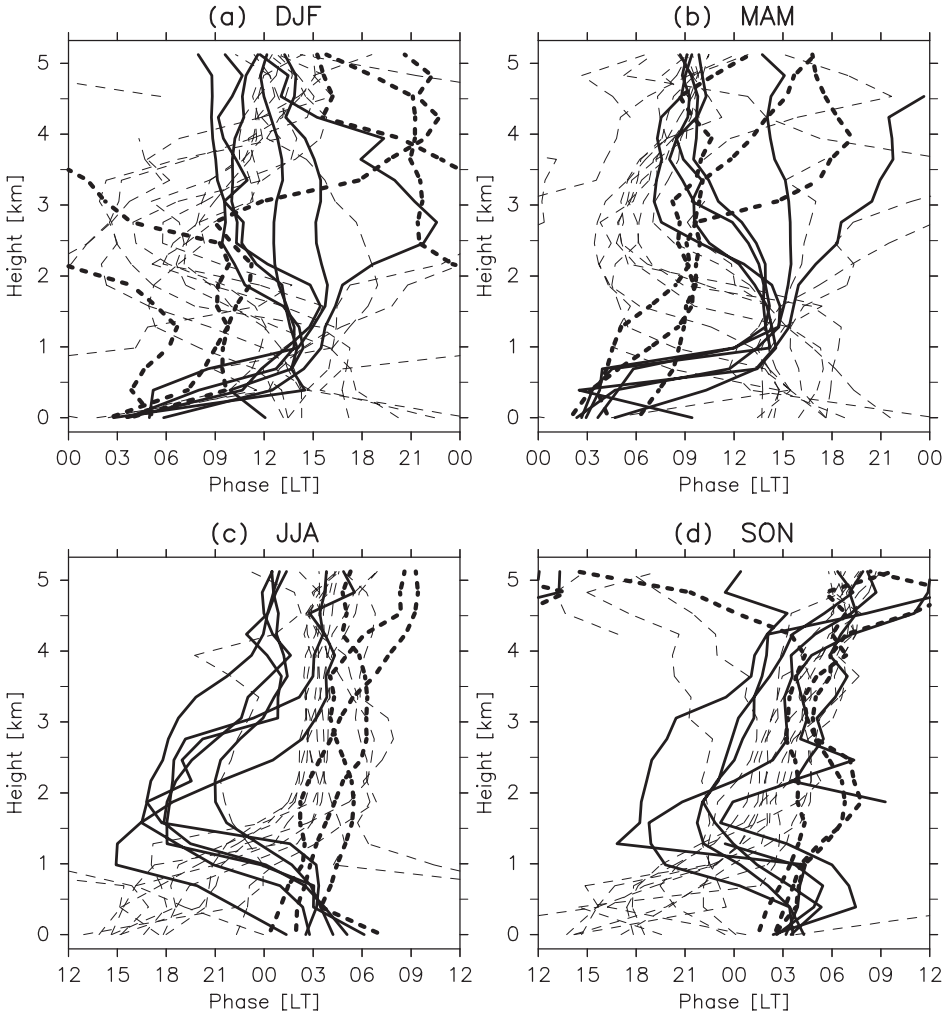

Fig. 11. Vertical profiles of the diurnal phase of v in (a) December–January–February (DJF), (b) March–April–May (MAM), (c) June–July–August (JJA), and (d) September–October–November (SON). Solid lines are for N-stations (stations 5, 6, 7, and 17–19), thin dashed lines are for S-stations (stations 2, 3, 9, 10, 12–16, 20, and 21), and thick dotted lines are for I-stations (stations 29–31). The center of the abscissa is 1200 LT for (a) and (b), and 0000 LT for (c) and (d). Data are not plotted in the case that the phase standard error exceeds 12 hr.

results, except that the phase of u is basically preceded by that of v, reflecting the clockwise rotation evident in the hodographs (Fig. 9).

We further examine the vertical phase structures at I-stations, as the wind system over these stations is identified as the diurnal tide over the entire lower troposphere throughout the year in Part II of this study. Figure 11 shows vertical profiles of diurnal phases of v for I-stations, as defined above. Note that the center of the abscissa in Fig. 11 is 1200 LT in DJF and MAM, and 0000 LT in JJA and SON. In DJF–MAM, the phase varies abruptly with height and the vertical wavelengths are estimated as 5–10 km. In contrast, in JJA–SON, the phase has a small positive slope, indicating downward energy propagation. The vertical wavelengths are estimated to be $\sim$20 km (the phase is $\sim$0300 LT at 0.0 km and $\sim$0900 LT at 5.0 km), being larger than those in DJF–MAM. According to tidal theory (Chapman and Lindzen 1970), the theoretical vertical wavelength of the principal Hough mode (first symmetric propagating mode) of the migrating diurnal tide is 25–30 km. The higher-order Hough modes of the migrating component

and nonmigrating components have small vertical wavelengths. In particular, the wavelengths of nonmigrating components due to planetary boundary layer sensible heating are reported to be 3–5 km (Tsuda and Kato 1989; Sasi et al. 1998). Thus, our observation results suggest that the diurnal component in JJA–SON is influenced mainly by the principal Hough mode of the migrating component, probably excited by radiative heating of water vapor and/or latent heat release; that in DJF–MAM is affected mainly by higher-order Hough modes of the migrating component and/or nonmigrating components. The excitation mechanism is further discussed in Part II of this study.

In summary, the characteristics of the diurnal wind component are different between the main Japanese islands and small southern islands. For the main Japanese islands, different phenomena prevail at the surface, at 1.9 km, and at 5.1 km. At the surface, the hodographs show winds that are primarily controlled by local wind systems (mainly land–sea breezes) throughout the year. At 1.9 km, the phase of the winds is reversed from that at the surface, indicating the dominance of the return currents of local wind systems. The amplitude of v is large along the north (south) coast in spring (autumn). Considering that local wind systems are strongest in summer, it is suggested that the winds are influenced not only by the return currents but by other disturbances; in other words, disturbances with a clear seasonal variation are superposed on the return currents, resulting in amplitude maxima in spring and autumn at 1.9 km. At 5.1 km, the wind system differs between DJF–MAM and JJA–SON. In DJF–MAM, an eastward phase delay is observed, indicating that eastward-moving disturbances control the diurnal wind component. In JJA–SON, the phase difference is small among the stations, indicating that the winds are influenced by the diurnal tide with a horizontal scale larger than the size of Japan. The differences in the dominant wind systems during JJA–SON and DJF–MAM generate the abrupt changes evident in April–May and November–December in the phase profile in Fig. 8.

Finally, over the entire lower troposphere, the diurnal component at I-stations located equatorward of 30°N is controlled by a different wind system to that over the main Japanese islands. At certain height levels and in some seasons, the phases are coherent with those over the main Japanese islands. The vertical wavelengths are small (5–10 km) in DJF–MAM and large ($\sim$20 km) in JJA–SON.

As a reference with which to compare our findings regarding the diurnal tide at 5.1 km, we analyze the diurnal tide at 4 km in the tidal model GSWM02. In GSWM02, the amplitude ranges from $\sim$0.1 m s^{-1} (45°N) to $\sim$0.5 m s^{-1} (25°N) for both u and v. For the region (20–50°N, 120–150°E), the phase of u (v) is 1800 (1200) LT, with no dependence on longitude or latitude throughout the year. Although the amplitude in GSWM02 is generally consistent with our results at 5.1 km, the phase is not, particularly over the main Japanese islands (Fig. 10).

5.3 Return currents and eastward-moving phenomena

a. Return currents

Here, we investigate the height range in which the local wind systems, including the return currents, influence the diurnal wind component. Figure 11 also shows vertical profiles of diurnal phases of v for N- and S-stations, as defined above. As mentioned above, we focus on the phase of v to clearly detect the signals of local wind systems.

At the surface, the winds are northward at 0000–0600 LT (1200–1800 LT) at N-stations (S-stations) throughout the year; that is, the winds are onshore in the afternoon and offshore early in the morning due to land–sea breezes at both N- and S-stations, as already shown in Section 5.2.a. This surface wind system extends up to 0.5–1 km, although the upper height increases to $\sim$1.5 km for S-stations in DJF–MAM because in these seasons, an eastward-moving disturbance at 1–3 km is in phase with the surface wind system along the south coast.

Above $\sim$1 km, the phases are reversed from those at the surface throughout the year. The winds are basically offshore in the afternoon and onshore during the early morning. Thus, for both N- and S-stations, the wind system at this height is interpreted as the return current of the local surface wind system.

Above 3–4 km, the phases at N- and S-stations approach each other, reaching 0900–1500 LT in DJF–MAM and 0000–0600 LT in JJA–SON. These phases correspond to the average phase for all stations at 4–5 km (Figs. 6d, 8, 10). Therefore, it is suggested that the return currents are confined to below 3–4 km and that other wind systems, with a horizontal scale greater than that of local wind

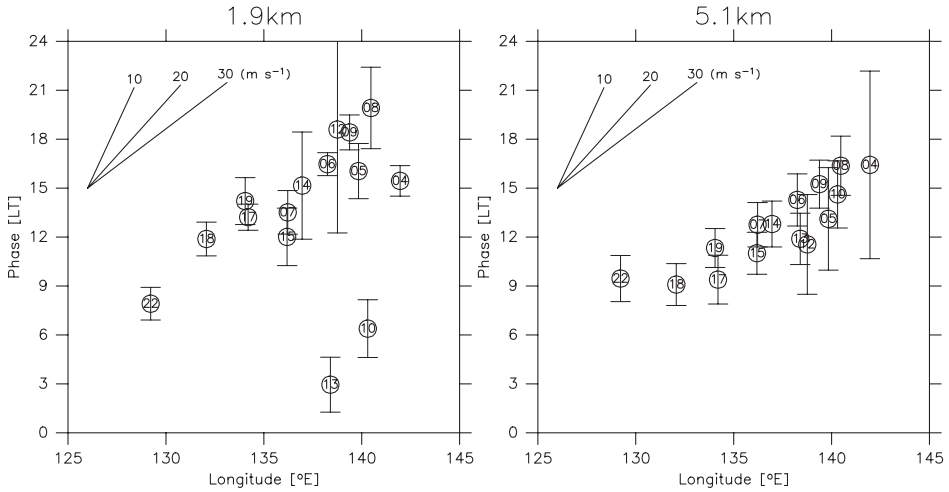

Fig. 12. Scatter plot of station longitude and diurnal phase of v for latitudes of 34°N–40°N in January–February–March. The numbers in circles represent station numbers. Vertical bars represent 95% confidence levels (t-test). Sloping lines indicate the reference eastward zonal phase speed.

systems (i.e., eastward-moving disturbances in DJF–MAM and diurnal tide in JJA–SON), prevail above 3–4 km. Therefore, the secondary amplitude peaks at 1–3 km (Fig. 6) are due in part to the return currents. The amplitude maximum in autumn (Fig. 7) is confined to the region of the return currents. The top height of the return currents is basically consistent with that reported in previous studies (e.g., Fujibe and Asai 1979; Oliphant et al. 2001).

In accordance with seasonal variations in the phase of large-scale wind systems above 3–4 km, the vertical structure of phases changes with the season. For example, in JJA, the phases above 1–2 km for S-stations have a vertically standing structure, because the return currents and large-scale wind system have the same phase (a typical example is seen at Kumagaya; Fig. 5b). In contrast, in DJF, the phases above 1–2 km for S-stations vary with height because of the contrasting phases of the return currents and the large-scale wind systems.

b. Eastward-moving phenomena

Here, we further examine the disturbance with an eastward phase delay observed in DJF–MAM at 1.9 and 5.1 km height (Fig. 10). Figure 12 shows scatterplots of station longitude versus the diurnal phase of v, at 1.9 and 5.1 km in January–February–March, when the phase delay is pronounced. Data are plotted for stations at latitudes of 34°N to 40°N. At both 1.9 and 5.1 km, we observe a disturbance that continuously propagates eastward from ~130°E to ~140°E. The corresponding eastward phase speed is ~20 m s^{-1} at 1.9 km and 20–30 m s^{-1} at 5.1 km. This phase propagation is largely observed in DJF–MAM for v, at both 1.9 and 5.1 km height. Note that this phase propagation is not clearly seen for u over the main Japanese islands throughout the year.

Figure 13 shows a time series of longitude–height distributions of the diurnal component of v, from 1200 JST to 2100 JST at 3-hour intervals in January–February–March. We use the data at stations 04–06, 07, 17, 18, and 22, which are located at approximately 35°N. v has a maximum (~0.8 m s^{-1}) at around 135°E at 1200 JST and 4–5 km. The maximum moves eastward and reaches 138°E at 1500 JST, when a line of zero velocity appears at 131°E and moves eastward to 137°E at 2100 JST. The corresponding phase speed is 25 m s^{-1}, consistent with the estimated phase velocity for 5.1 km in Fig. 12. Note that this eastward-moving phenomenon shows a barotropic structure, with its amplitude increasing with height. These characteristics (i.e., zonal phase speed and vertical structure) are consistent with those of the medium-scale eastward-traveling waves reported by Sato et al. (1993). Therefore, it is suggested that these medium-scale waves contribute to the diurnal wind component above 3–4 km over Japan in DJF–MAM and that the maximum amplitude in Febru-

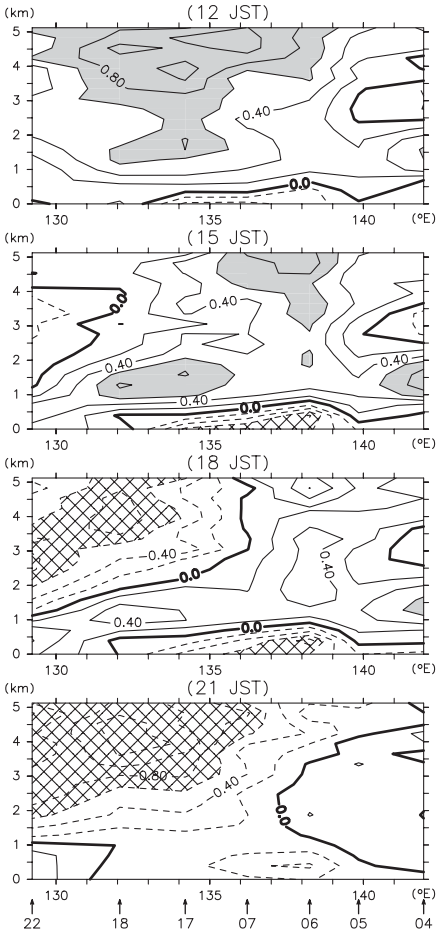

Fig. 13. Longitude–height distributions of the diurnal component of v from 1200 JST to 2100 JST at 3-hour intervals in January–February–March from selected stations located at approximately ∼35°N. The longitudes of the selected stations are denoted by the vectors below the bottom panel, which are accompanied by the relevant station numbers. The contour interval is 0.2 m s^{-1}. The regions with >0.6 m s^{-1} (<−0.6 m s^{-1}) are colored gray (hatched).

ary above 3–4 km (Fig. 7) is caused by this phenomena. The eastward signals at 1.9 km in Fig. 13 are not clearly seen in Fig. 10, but are discussed as an independent mode, Diurnal Eastward-moving Eddies (DEEs), in Part II of this study.

6. Results and discussion on the semidiurnal wind component

Figure 14 shows vertical profiles of semidiurnal amplitudes for each season. The amplitude is 0.2∼0.5 m s^{-1} for both u and v, and is near-constant with height throughout the year. The amplitudes are slightly smaller than those of the diurnal wind component (Figs. 5, 6). The SD is <0.2 m s^{-1} in DJF and <0.1 m s^{-1} in JJA, again smaller than that for the diurnal component. Figure 15 shows the month–height distributions of the semidiurnal amplitude averaged for all stations. Unlike the diurnal component (Fig. 7), the amplitude is small near the surface. There exists a marked seasonal variation above 2–3 km for both u and v, with maxima of 0.4–0.5 m s^{-1} in winter and minima of 0.2–0.3 m s^{-1} in summer.

Figure 14 also shows vertical profiles of semidiurnal phases for each season. The differences among the stations are minor above ∼1 km. The SD is >3 hr at the surface and <1 hr above 1 km, except for some levels in some months for u. The average phase of u (v) has a constant value of ∼0400 LT (0100 LT) regardless of height, indicating that the meridional component precedes the zonal component by a quadrature, and that the semidiurnal wind vector rotates clockwise in a horizontal plane. Furthermore, there is little seasonal variation in phase, in contrast to the diurnal wind component (Figs. 6, 8).

Chapman and Lindzen (1970) predicted the phase of the migrating semidiurnal tide based on observation data of diurnal pressure tide (see also Whiteman and Bian 1996). The authors showed that the semidiurnal phase of u is 0344 LT in both hemispheres, while that of v is 0044 LT (0644 LT) in the Northern (Southern) Hemisphere. The phases obtained in the present study, 0400 LT (0100 LT) for u (v), are similar to those predicted; the GSWM02 results are also consistent with the present findings. Furthermore, according to tidal theory (Chapman and Lindzen, 1970), the vertical wavelength of the semidiurnal tide is relatively long (∼200 km) and the vertical phase tilt is relatively small. Again, the present results are consistent with this theoretical prediction (Fig. 14c, d). Therefore, we conclude that the semidiurnal component above ∼1 km over Japan is caused by the semidiurnal migrating tide throughout the year. The semidiurnal amplitudes reported in this study (0.2–0.5 m s^{-1}) are consistent with those in the lower troposphere over the USA (0.2–0.5 m s^{-1}) (Fig. 8 in Whiteman and Bian 1996), but larger than those in the tropics (∼0.2 m s^{-1}) (Williams et al. 1992). The occurrence of larger amplitudes in midlatitude regions is consistent with the theoretical prediction

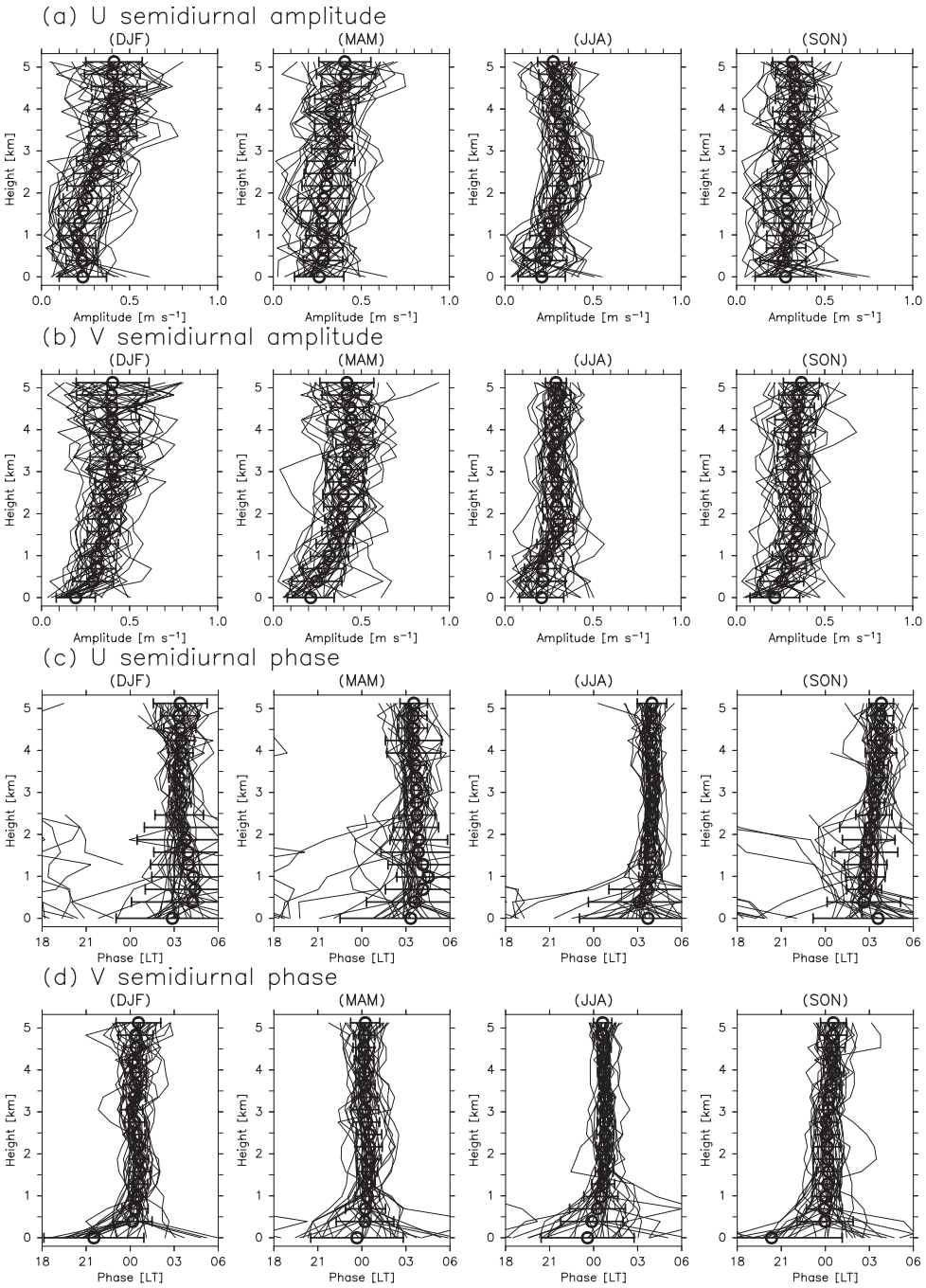

Fig. 14. As for Fig. 6, but for the semidiurnal wind component. For (c) and (d), data are not plotted in the case that SE exceeds 6 hr.

that the semidiurnal migrating tidal winds have maximum amplitudes in subtropical to midlatitude regions (20–30°) (Figs. 3.4 and 3.5 in Chapman and Lindzen 1970).

Based on the above results, the seasonal variation in semidiurnal amplitudes shown in Fig. 15 is regarded as that of the semidiurnal tide. A marked seasonal variation in amplitude is seen in GSWM02, although qualitatively rather than quantitatively; the amplitudes in GSWM02 at 4 km

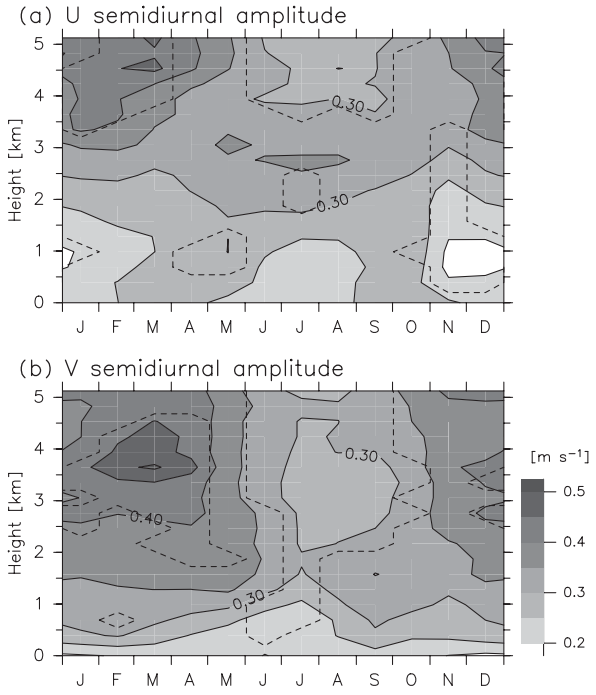

Fig. 15. As for Fig. 7, but for the semidiurnal wind component.

show a maximum of $\sim$0.16 m s^{-1} in winter and a minimum of $\sim$0.13 m s^{-1} in summer. The winter (summer) maxima are approximately 33% (50%) smaller than the present results. Iwai and Miyashita (2005) found that the amplitude of semidiurnal surface pressure over Japan attains a maximum (0.6–0.9 hPa) in winter and a minimum in summer (0.4–0.6 hPa). These seasonal variations are probably related to that in ozone distribution, which is considered the main source of the semidiurnal tide (Chapman and Lindzen 1970).

Below $\sim$1 km, large differences are observed among stations, particularly in terms of phase. These differences reflect the semidiurnal wind component of local wind systems, as discussed by Sakazaki and Fujiwara (2008). In fact, the amplitude of $\sim$0.2 m s^{-1} (Fig. 15) is consistent with the finding of Sakazaki and Fujiwara (2008) that the semidiurnal amplitude associated with the local wind system is approximately one-third smaller than that of the diurnal component (in the present study, the diurnal amplitudes below 1 km, which are largely due to the local wind system, are 0.6–0.8 m s^{-1} (Fig. 7)). Thus, it is concluded that for the semidiurnal wind component, the influence of local wind systems extends up to $\sim$1 km.

7. Concluding remarks

We studied diurnal variations in lower-tropospheric wind between the surface and $\sim$5 km over Japan, using WINDAS and AMeDAS data from 31 WINDAS stations. The diurnal and semidiurnal harmonic components were extracted from the local time composite of the horizontal wind data, and were analyzed for each height range and for each season.

For the diurnal wind component, the amplitude averaged for all stations attains a maximum of ($\sim$0.8 m s^{-1}) in JJA near the surface. At 1–3 km, the average amplitude is largest in autumn ($\sim$0.6 m s^{-1}), followed by spring ($\sim$0.5 m s^{-1}); the average amplitude is relatively small in summer and winter. At 3–5 km, the average amplitude is largest in February, with the amplitude of v ($\sim$0.8 m s^{-1}) being larger than that of u ($\sim$0.4 m s^{-1}). In addition, for the entire height region, the average phase shows a clear seasonal variation. The average phase of u (v) below 5 km is 1500–2100 LT (1200–1500 LT) in DJF and 0300–0900 LT (0000–0400 LT) in JJA, with abrupt changes in spring and autumn.

Analysis of hodographs and harmonic dial vectors revealed that for the diurnal wind component, the dominant wind system is different between the main Japanese islands and small southern islands. For the main Japanese islands, the surface winds are controlled by local wind systems, as discussed previously by Sakazaki and Fujiwara (2008). The strength of the surface wind system is greatest in summer. At 1–3 km, the autumn maximum tends to appear at stations along the south coast of the main Japanese islands, while the spring maximum is found at stations along the north coast. The return currents of the surface wind systems (local wind systems) prevail throughout most of the year in this height region; however, other larger-scale disturbances also affect the diurnal winds, particularly in spring and autumn. The larger-scale disturbances strengthen the return currents along the north (south) coast of the main Japanese islands in spring (autumn) because of a favorable phase relation. This superposition results in the spring and autumn amplitude maxima. Furthermore, in winter and spring, these disturbances show an eastward phase propagation of $\sim$20 m s^{-1} over the main Japanese islands. Finally, at 3–5 km in DJF–MAM, we suggest that the diurnal wind component of v at 3–5 km is caused mainly by medium-

scale eastward-traveling waves with a phase speed of $\sim$25 m s^{-1} and maximum amplitude located in the upper troposphere (Sato et al. 1993). These waves result in large amplitudes at 3–5 km in February. At 3–5 km in JJA–SON, the diurnal wind is caused by a large-scale wind system with a horizontal scale larger than the scale of Japan ($\sim$3000 km); the amplitudes are 0.3–0.4 m s^{-1}. This large-scale wind system is caused by atmospheric tides, although the tidal phase in the tidal model GSWM02 at 4 km is not consistent with our results.

At stations located on small southern islands equatorward of $\sim$30°N, the wind system is different from that at stations on the main Japanese islands throughout the year, with amplitudes of 0.2–0.4 m s^{-1} over the lower troposphere in all seasons. The vertical wavelengths are small (5–10 km) in DJF–MAM and large ($\sim$20 km) in JJA–SON.

For the semidiurnal component, the difference in amplitudes and phases among the WINDAS stations is relatively small above $\sim$1 km and large below $\sim$1 km. Above $\sim$1 km, the phase of v (0100 LT) precedes that of u (0400 LT) by a quadrature, and the phase is approximately constant with height; these observations are consistent with classical tidal theory regarding the semidiurnal migrating tide, as proposed by Chapman and Lindzen (1970). Therefore, we conclude that the semidiurnal migrating tide is dominant above $\sim$1 km. The semidiurnal amplitude attains a maximum in winter (0.4–0.5 m s^{-1}) and a minimum (0.2–0.3 m s^{-1}) in summer. Below $\sim$1 km, the semidiurnal wind component is attributed to local wind systems, as discussed by Sakazaki and Fujiwara (2008).

Thus, diurnal variations in lower-troposphere wind are influenced by at least three phenomena other than the local wind systems, including their return currents. The first is an eastward-moving disturbance with a zonal phase velocity of $\sim$20 m s^{-1} at 1–3 km in DJF–MAM, which is superposed on the return currents. The second is an eastward-moving disturbance with a phase velocity of $\sim$25 m^{-1}s at 3–5 km in winter–spring. The third is a large-scale wind system (>3000 km) at 3–5 km in summer–autumn. In Part II of this study, based on meso-scale analysis data and global reanalysis data, these three phenomena are identified as diurnal eastward-traveling eddies (DEEs), medium-scale eastward-traveling waves, and the diurnal tide, respectively. In addition, the diurnal wind system at small southern islands is identified as the diurnal tide, over the entire lower troposphere.

When using horizontal wind data sampled diurnally in the lower troposphere, it is important to consider the bias due to diurnal variations with amplitudes of up to $\sim$1.0 m s^{-1} (the sum of diurnal and semidiurnal amplitudes), although the bias depends on location, season, and height range.

Acknowledgments

WINDAS and AMeDAS data were provided by the Japan Meteorological Agency (JMA), and GSWM02 data were provided by Dr. Maura Hagan through the Web site http://www.hao.ucar.edu/public/research/tiso/gswm/gswm.html. This work was supported by the JSC-S Scholarship Foundation, and by the Japanese Ministry of Education, Culture, Sports, Science and Technology (MEXT) through Grants-in-Aid for Scientific Research (2200295800). We wish to express our gratitude to Dr. Koji Yamazaki for useful advice regarding the interpretation of daily-mean winds. We thank Dr. Fumio Hasebe for useful advice regarding statistical significance tests in composite analysis. We are also grateful to Dr. Isamu Hirota and two anonymous reviewers for their helpful comments and suggestions. All figures were drawn using the GFD-DENNOU Library.

References

Alexander, S. P., and T. Tsuda, 2008: Observations of the diurnal tide during seven intensive radiosonde campaigns in Australia and Indonesia. *J. Geophys. Res.*, **113**, D04109, doi:10.1029/2007JD008717.

Chapman, S., and R. S. Lindzen, 1970: *Atmospheric Tides.*, D. Reidel Publ. Co., 200 pp.

Chen, T.-C. (M.), M.-C. Yen, and R. Arritt, 1998: Detection of semidiurnal wind oscillations with a radar profiler. *Bull. Amer. Meteor. Soc.*, **79**, 1921–1924.

Eady, E. T., 1949: Long waves and cyclonic waves. *Tellus*, **1**, 33–52.

Forbes, J. M., M. E. Hagan, X. Zhang, and K. Hamilton, 1997: Upper atmosphere tidal oscillations due to latent heat release in the tropical troposphere. *Ann. Geophys.*, **15**, 1165–1175.

Fujibe, F., and T. Asai, 1979: A study of local winds in Kanto district. Part I: Structures of wind systems with diurnal variation. *Tenki*, **26**, 595–604 (in Japanese).

Gill, A. E., 1980: Some simple solutions for heat-induced tropical circulation. *Quart. J. Roy. Meteor. Soc.*, **106**, 447–462.

Hagan, M. E., J. M. Forbes, and F. Vial, 1995: On mod-

eling migrating solar tides. *Geophys. Res. Lett.*, **22**, 893–896.

Hagan, M. E., M. D. Burrage, J. M. Forbes, J. Hackney, W. J. Randel, and X. Zhang, 1999: GSWM-98: Results for migrating solar tides. *J. Geophys. Res.*, **104(A4)**, 6,813–6,827.

Hagan, M. E., and J. M. Forbes, 2002: Migrating and nonmigrating diurnal tides in the middle and upper atmosphere excited by tropospheric latent heat release. *J. Geophys. Res.*, **107(D24)**, 4754, doi:10.1029/2001JD001236.

Hagan, M. E., and J. M. Forbes, 2003: Migrating and nonmigrating semidiurnal tides in the upper atmosphere excited by tropospheric latent heat release. *J. Geophys. Res.*, **108(A2)**, 1062, doi:10.1029/2002JA009466.

Hamilton, K., 1981: Latent heat release as a possible forcing mechanism for atmospheric tides. *Mon. Wea. Rev.*, **109**, 3–17.

Hashiguchi, H., S. Fukao, Y. Moritani, T. Wakayama, and S. Watanabe, 2004: A lower troposphere radar: 1.3-GHz active phased-array type wind profiler with RASS. *J. Meteor. Soc. Japan*, **82**, 915–931.

Held, I. M., 1983: Stationary and quasi-stationary eddies in the extratropical tropopause: theory. *Large-Scale Dynamical Processes in the Atmosphere.*, ed. B. J. Hoskins and R. Pearce, Academic Press, 127–168.

Hsu, H.-H., and B. J. Hoskins, 1989: Tidal fluctuations as seen in ECMWF data. *Quart. J. Roy. Meteor. Soc.*, **115**, 247–264.

Ishihara, M., Y. Kato, T. Abo, K. Kobayashi, and Y. Izumikawa, 2006: Characteristics and performance of the operational wind profiler network of the Japan Meteorological Agency. *J. Meteor. Soc. Japan.*, **84**, 1085–1096.

Iwai, K., and E. Miyashita, 2005: Diurnal, semi-diurnal and ter-diurnal pressure variations at the stations of central mountain area of Japan. *Tenki*, **52**, 831–836 (in Japanese).

Kodama, Y.-M., K. Egawa, and M. Takahashi, 2008: Medium-scale tropopausal waves visualized by upper-level clouds to the east of Tibetan Plateau. *J. Meteor. Soc. Japan*, **86**, 279–295.

Kurita, H., H. Ueda, and S. Mitsumoto, 1990: Combination of local wind systems under light gradient wind conditions and its contribution to the long-range transport of air pollutants. *J. Appl. Meteor.* **29**, 331–348.

Lieberman, R. S., and C. B. Leovy, 1995: A numerical model of nonmigrating diurnal tides between the surface and 65 km. *J. Atmos. Sci.*, **52**, 389–409.

Matsuno, T., 1966: Quasi-geostrophic motions in the equatorial area. *J. Meteor. Soc. Japan*, **44**, 25–43.

Miller, S. T. K., B. D. Keim, R. W. Talbot, and H. Mao, 2003: Sea breeze: Structure, forecasting, and impacts. *Rev. Geophys.*, **41(3)**, 1011, doi:10.1029/2003RG000124.

Oliphant, A. J., A. P. Sturman, and N. J. Tapper, 2001: The evolution and structure of a tropical island sea/land-breeze system, northern Australia. *Meteor. Atmos. Phys.*, **78**, 45–59.

Onogi, K., J. Tsutsui, H. Koide, M. Sakamoto, S. Kobayashi, H. Hatsushika, T. Matsumoto, N. Yamazaki, H. Kamahori, K. Takahashi, S. Kadokura, K. Wada, K. Kato, R. Oyama, T. Ose, N. Mannoji, and R. Taira, 2007: The JRA-25 reanalysis. *J. Meteor. Soc. Japan*, **85**, 369–432.

Riggin, D. M., E. Kudeki, Z. Feng, M. F. Sarango, and R. S. Lieberman, 2002: Jicamarca radar observations of the diurnal and semidiurnal tide in the troposphere and lower stratosphere. *J. Geophys. Res.*, **107(D8)**, doi:10.1029/2001JD001216.

Sakazaki, T., and M. Fujiwara, 2008: Diurnal variations in summertime surface wind upon Japanese plains: Hodograph rotation and its dynamics. *J. Meteor. Soc. Japan*, **86**, 787–803.

Sakazaki, T., and M. Fujiwara, 2010: Diurnal variations in lower-tropospheric wind over Japan. Part II: Analysis of Japan Meteorological Agency mesoscale analysis data and four global reanalysis data sets. *J. Meteor. Soc. Japan*, **88**, 349–372.

Sasi, M. N., G. Ramkumar, and V. Deepa, 1998: Nonmigrating diurnal tides in the troposphere and lower stratosphere over Gadanki (13.5°N, 79.2°E). *J. Geophys. Res.*, **103(D16)**, 19,485–19,494.

Sasi, M. N., G. Ramkumar, and V. Deepa, 2001: Tidal wind oscillations in the tropical lower atmosphere as observed by Indian MST radar. *Ann. Geophys.*, **19**, 991–999.

Sato, K., H. Eito, and I. Hirota, 1993: Medium-scale travelling waves in the extra-tropical upper troposphere. *J. Meteor. Soc. Japan*, **71**, 427–436.

Sato, K., K. Yamada, and I. Hirota, 2000: Global characteristics of medium-scale tropopausal waves observed in ECMWF operational data. *Mon. Wea. Rev.*, **128**, 3808–3823.

Seidel, D. J., M. Free, and J. Wang, 2005: Diurnal cycle of upper-air temperature estimated from radiosondes. *J. Geophys. Res.*, **110**, D09102, doi:10.1029/2004JD005526.

Tijm, A. B. C., A. A. N. Holtslag, and A. J. van Delden, 1999: Observations and modeling of the sea breeze with the return current. *Mon. Wea. Rev.*, **127**, 625–640.

Tokioka, T., and I. Yagai, 1987: Atmospheric tides appearing in a global atmospheric general circulation model. *J. Meteor. Soc. Japan*, **65**, 423–437.

Tomikawa, Y., K. Sato, and T. G. Shepherd, 2006: A diagnostic study of waves on the tropopause. *J. Atmos. Sci.*, **63**, 3315–3332.

Tsuda, T., and S. Kato, 1989: Diurnal non-migrating

tides excited by a differential heating due to land-sea distribution. *J. Meteor. Soc. Japan*, **67**, 43–55.

Tsuda, T., Y. Murayama, H. Wiryosumarto, S. W. B. Harijono, and S. Kato, 1994: Radiosonde observations of equatorial atmosphere dynamics over Indonesia 1. Equatorial waves and diurnal tides. *J. Geophys. Res.*, **99(D5)**, 10,491–10,505.

Wallace, J. M., and F. R. Hartranft, 1969: Diurnal wind variations, surface to 30 kilometers. *Mon. Wea. Rev.*, **97**, 446–455.

Wallace, J. M., and R. F. Tadd, 1974: Some further results concerning the vertical structure of atmospheric tidal motions within the lowest 30 kilometers. *Mon. Wea. Rev.*, **102**, 795–803.

Whiteman, C. D., and X. Bian, 1995: Radar wind profiler observations of solar semidiurnal atmospheric tides. *Geophys. Res. Lett.*, **22**, 901–904.

Whiteman, C. D., and X. Bian, 1996: Solar semidiurnal tides in the troposphere: Detection by radar profilers. *Bull. Amer. Meteor. Soc.*, **77**, 529–542.

Williams, C. R., and S. K. Avery, 1996a: Diurnal nonmigrating tidal oscillations forced by deep convective clouds. *J. Geophys. Res.*, **101(D2)**, 4079–4091.

Williams, C. R., and S. K. Avery, 1996b: Diurnal winds observed in the tropical troposphere using 50 MHz wind profilers. *J. Geophys. Res.*, **101(D10)**, 15,051–15,060.

Williams, C. R., S. K. Avery, J. R. NcAfee, and K. S. Gage, 1992: Comparison of observed diurnal and semidiurnal tropospheric winds at Christmas island with tidal theory. *Geophys. Res. Lett.*, **19**, 1471–1474.

Yamamori, M., K. Sato, and I. Hirota, 1997: A study on seasonal variation of upper tropospheric medium-scale waves over East Asia based on regional climate model data. *J. Meteor. Soc. Japan*, **75**, 13–22.

Yoshida, A., and I. Hirota, 1979: Diurnal wind variation in the troposphere and lower stratosphere over Japan. *J. Meteor. Soc. Japan*, **57**, 29–38.